

WMAP-normalized Inflationary Model Predictions and the Search for Primordial Gravitational Waves with Direct Detection Experiments

Brett C. Friedman, Asantha Cooray

*Center for Cosmology, Dept. of Physics & Astronomy,
University of California, Irvine, CA 92697-4575*

Alessandro Melchiorri

*Dipartimento di Fisica “G. Marconi” and INFN, sezione di Roma,
Universita’ di Roma “La Sapienza”, Ple Aldo Moro 5, 00185, Roma, Italy.*

In addition to density perturbations, inflationary models of the early universe generally predict a stochastic background of gravitational waves or tensor fluctuations. By making use of the inflationary flow approach for single field models and fitting the models with Monte-Carlo techniques to cosmic microwave background (CMB) data from the *Wilkinson Microwave Anisotropy Probe* (WMAP), we discuss the expected properties of the gravitational wave background from inflation at scales corresponding to direct detection experiments with laser interferometers in space. We complement the Monte-Carlo numerical calculations by including predictions expected under several classes of analytical inflationary models. We find that an improved version of *Big Bang Observer* (BBO-grand) can be used to detect a gravitational wave background at 0.1 Hz with a corresponding CMB tensor-to-scalar ratio above 10^{-4} . Even if the CMB tensor-to-scalar ratio were to be above 10^{-2} , we suggest that BBO-grand will be useful to study inflationary models as the standard version of BBO, with a sensitivity to a stochastic gravitational wave background $\Omega_{\text{GW}} h^2 > 10^{-17}$, will only allow a marginal detection of the amplitude while leaving the tensor spectral index at 0.1 Hz unconstrained. Also, inflationary models with a large tensor-to-scalar ratio predict a substantial negative tensor spectral index such that the gravitational wave amplitude is damped at direct detection frequencies. We also discuss the extent to which CMB measurements can be used to predict the gravitational wave background amplitude in a direct detection experiment and how any measurement of the amplitude and the spectral tilt of the gravitational wave background at direct detection frequencies together with the CMB tensor-to-scalar ratio can be used to establish slow-roll inflation.

PACS numbers: 98.80.Bp, 98.80.Cq, 04.30.Db, 04.80.Nn

I. INTRODUCTION

The data from high precision cosmological experiments relating cosmic microwave background (CMB) radiation [1] and large-scale structure mass distribution from galaxy redshift surveys have clearly demonstrated that the inflationary paradigm [2] is the most preferred description of the origin of density perturbations. While expectations are generally consistent with existing observations, we still lack a complete understanding of underlying physics related to inflation including the shape and the amplitude of the potential responsible for superluminal expansion.

The cosmological observations, so far, have been restricted to studying the density, or scalar, fluctuations in the universe both through CMB and large-scale structure. In addition to scalar perturbations, tensor fluctuations in the form of a primordial gravitational wave background are expected to be generated during inflation [3]. If detected, the amplitude of the gravitational wave background provides a direct estimate of the potential height of the inflaton field when relevant modes exit the horizon. This background is now the focus of a large number of ongoing and upcoming CMB polarization experiments since gravitational waves leave a distinct signature in the polarization pattern of CMB photons in

the form of B- or curl-modes [4]. The *Wilkinson Microwave Anisotropy Probe* (WMAP; [5]) data have now constrained the the tensor-to-scalar ratio, r_{CMB} , denoting the tensor power spectrum amplitude divided by the amplitude of the scalar perturbation power spectrum, to be below 0.38 at CMB scales (at 95% confidence level [6]).

The planned next generation NASA mission for high precision polarization observations (*CMBpol* or *Inflation Probe*) has now set a detection goal for r_{CMB} above 10^{-2} [7]. In the future, with an ambitious experiment, this limit could be further improved, though confusion from known polarized foregrounds involving dust and synchrotron will limit CMB studies to a level above a few times 10^{-4} [8]. While all-sky maps of polarized synchrotron emission are now available with low-frequency channels of WMAP, the aforementioned uncertainty is due to the lack of all-sky maps at frequencies dominated by polarized dust. With data from Planck, it is very likely that we will have a more exact estimate on the limit to which a tensor background can be probed with next generation CMB polarization experiments. It is now clear that the limiting factor for CMB observations is not the ultimate lensing confusion that was previously discussed in the literature with a minimum detectable tensor-to-scalar ratio around 10^{-5} [9].

Beyond CMB, there is now a growing interest to directly detect the relic gravitational wave background from inflation with laser interferometers in space with test masses separated by a few thousand to 50,000 kilometers. Plans for such studies include NASA's *Big Bang Observer* (BBO) [10] and the *DECI-hertz Interferometer Gravitational Wave Observatory* (DECIGO) in Japan [11]. Other studies that explore possibilities for future gravitational wave observations beyond first generation *Laser Interferometer Space Antenna* can be found in Ref. [12]. Based on the expected foreground confusion and technological improvements, current concept studies aim the frequency regime between 0.1 Hz to a few Hz [18]. Here we will use 0.1 Hz with a corresponding scale $k \sim 6.47 \times 10^{13} \text{ Mpc}^{-1}$ as the fiducial frequency for direct detection experiments. As CMB measurements are sensitive to density and tensor perturbations at horizon-size scales, at $k \sim 0.002 \text{ Mpc}^{-1}$, the two detection techniques are roughly sensitive to a gravitational wave background at wavelengths separated by 16 orders of magnitude.

As discussed in a variety of recent papers [13, 14, 15, 16, 17], the large lever arm produced by combining information at CMB and direct detection scales is expected to pin down inflationary models better than data from any one of the two scales alone. Recent studies have discussed the expected signal for direct detections either through exact calculations using specific analytic models [15] or through the use of numerically generated Monte-Carlo models [16, 17] under the inflationary flow equations [20, 21]. While general predictions exist and the expected level of the background is understood in terms of the CMB tensor-to-scalar ratio, past studies have paid little attention to issues of connecting CMB information with the gravitational wave background data at direct detection frequencies to improve inflationary models. While the long lever arm connecting the two scales has been advocated to help discern inflationary model space, as we discuss here, such a large lever arm also complicates a simple analysis based on a power-law extrapolation of tensor and scalar power spectra from CMB scales at $k = 0.002 \text{ Mpc}^{-1}$ to direct detection at $k = 6.47 \times 10^{13} \text{ Mpc}^{-1}$.

Furthermore, while past studies have discussed the possibility for a direct detection of the inflationary background with future laser interferometers [26], the sensitivity requirements for a direct detection experiment have not been fully characterized. We will try to determine how sensitive direct detection experiments will need to be and put these sensitivities in context with CMB polarization measurements. We also extend previous analysis that only concentrated on the gravitational wave background amplitude [17] to also discuss the detectability of the tensor spectral index at these frequencies. Our discussion is similar in spirit to the recent study in Ref. [16], but we improve the analysis by considering both numerical as well as analytical [15] models of inflation, combining separate analyses in the literature into a single discussion.

The combination of the tensor amplitude and the tilt can be used to validate inflationary models as these observables are expected to satisfy certain consistency relations. Similar tests are discussed at CMB scales in the literature, though these relations are poorly constrained due to the fact that tensor tilt is generally hard to measure at CMB scales [27]. As an application of our models, we extend the discussion in Smith et al. [16] to consider the possibility to test the inflationary consistency relation. This is done in Smith et al. under the assumption that one can use the tensor tilt from direct detection experiments as a proxy for the tensor tilt at CMB scales. Using numerical models, we show that for general inflaton potentials the tensor tilt at $k = 6.47 \times 10^{13} \text{ Mpc}^{-1}$ differs from the tensor tilt at $k = 0.002 \text{ Mpc}^{-1}$ by more than a factor of ten. Furthermore, beyond simply using a direct detection experiment to confirm a detection of tensor modes at CMB scales and thereby improve inflationary model selection, we also explore the usefulness of a highly sensitive direct detection experiment that is also capable of measuring the tensor tilt at direct detection frequencies. Unfortunately, while experiments such as ultimate-DECIGO can reach gravitational wave background amplitudes with the corresponding CMB tensor-to-scalar ratio of 10^{-6} and above, tensor tilt will remain unconstrained for most of the models with CMB tensor-to-scalar ratios below 10^{-3} and tilts with magnitude such that $|n_T| < 0.01$.

This paper is organized as follows: In the next Section, we outline our calculations that we use to predict properties of the gravitational wave background from inflationary models. We consider two separate approaches, one involving Monte-Carlo models of the inflationary flow equations, and the second using analytical families of inflationary models that are consistent with observations at CMB scales. In Section III, we discuss our results and comment on the sensitivity requirements for a direct detection experiment to reach similar sensitivities as those expected with CMB polarization observations. We conclude with a summary of our main results in Section IV.

II. CALCULATIONAL METHOD

A. Monte-Carlo Reconstruction of Inflationary Flows

To model the evolution of single field inflationary models, we study dynamics through the hierarchy of flow equations involving the generalized “Hubble Slow Roll” (HSR) parameters [20, 21, 22]. The advantage of the inflationary flow method is that one can study the generic behavior of the inflaton field without assuming a particular shape for the potential. We outline the main equations of this approach here and refer the reader to Refs. [21, 22] for further details.

To begin, we note that the motion of the scalar field in a cosmological background is given by $\ddot{\phi} + 3H\dot{\phi} + V'(\phi) =$

0 where an overdot corresponds to the time derivative, a prime denotes the derivative with respect to ϕ and $H \equiv (\dot{a}/a)$ is the Hubble parameter. Assuming the inflaton field dominates the energy density, the Einstein field equations are

$$\begin{aligned} H^2 &= \frac{8\pi}{3M_{\text{pl}}^2} \left[V(\phi) + \frac{1}{2}\dot{\phi}^2 \right] \\ \left(\frac{\ddot{a}}{a} \right) &= \frac{8\pi}{3M_{\text{pl}}^2} \left[V(\phi) - \dot{\phi}^2 \right]. \end{aligned} \quad (1)$$

As discussed in Refs. [23], the equations of motion can be written as

$$\begin{aligned} \dot{\phi} &= -\frac{M_{\text{pl}}^2}{4\pi} H'(\phi) \\ [H'(\phi)]^2 &= \frac{12\pi}{M_{\text{pl}}^2} H^2(\phi) - \frac{32\pi^2}{M_{\text{pl}}^4} V(\phi), \end{aligned} \quad (2)$$

where the Hubble parameter is now a function of the field ϕ instead of time under the assumption that ϕ varies monotonically with time.

As usual, dynamics are described in terms of the HSR parameters that are defined in terms of the derivatives of H with respect to ϕ [24]:

$$\begin{aligned} \epsilon(\phi) &\equiv \frac{M_{\text{pl}}^2}{4\pi} \frac{[H'(\phi)]^2}{H^2(\phi)} \\ {}^{\ell}\lambda_H &\equiv \left(\frac{M_{\text{pl}}^2}{4\pi} \right)^{\ell} \frac{(H')^{\ell-1}}{H^{\ell}} \frac{d^{(\ell+1)}H}{d\phi^{(\ell+1)}}, \quad (\ell \geq 1) \end{aligned} \quad (3)$$

and for comparison with similar calculations in the literature [17, 20, 21, 22] we identify the slow roll parameters ${}^1\lambda_H$ and ${}^2\lambda_H$ as η and ξ , respectively. We also define $\sigma \equiv 2\eta - 4\epsilon$.

The trajectories of these HSR parameters are governed by a set of coupled first order differential equations [20, 21] written in terms of the number of e-folds, N , before the end of inflation, with the convention that N increases as one goes further back in time, as

$$\begin{aligned} \frac{d\epsilon}{dN} &= \epsilon(\sigma + 2\epsilon) \\ \frac{d\sigma}{dN} &= -5\epsilon\sigma - 12\epsilon^2 + 2\xi \\ \frac{d({}^{\ell}\lambda_H)}{dN} &= \left[\frac{\ell-1}{2}\sigma + (\ell-2)\epsilon \right] ({}^{\ell}\lambda_H) + ({}^{\ell+1}\lambda_H) \quad (\ell > 1). \end{aligned} \quad (4)$$

As written, the evolution of a given slow roll parameter depends on a slow roll parameter that is one order higher. While the coupled differential equations involve an infinite hierarchy, in practice, this hierarchy must be truncated at some order M such that ${}^{M+1}\lambda_H = 0$. From Eq. 3, with $d^{(M+2)}H/d\phi^{(M+2)} = 0$, one can then write $H(\phi)$ as a polynomial of order $M+1$ with [25]

$$H(\phi) = H_0 \left[1 + A_1 \left(\frac{\phi}{M_{\text{pl}}} \right) + \dots + A_{M+1} \left(\frac{\phi}{M_{\text{pl}}} \right)^{M+1} \right]. \quad (5)$$

Further, from the definition of $\epsilon(\phi)$, one can also write [25]

$$\begin{aligned} \epsilon(\phi) &= \frac{M_{\text{pl}}^2}{4\pi} \\ &\times \left[\frac{(A_1/M_{\text{pl}}) + \dots + (M+1)(A_{M+1}/M_{\text{pl}})(\phi/M_{\text{pl}})^M}{1 + A_1(\phi/M_{\text{pl}}) + \dots + A_{M+1}(\phi/M_{\text{pl}})^{M+1}} \right]^2, \end{aligned} \quad (6)$$

when the coefficients A_i , with $i > 1$, are related to initial values of HSR parameters

$$A_{\ell+1} = \frac{(4\pi)^{\ell} \ell \lambda_{H,0}}{(\ell+1)! A_1^{\ell-1}}, \quad (7)$$

with $A_1 = \sqrt{4\pi\epsilon_0}$ and the sign of A_1 determining the direction the field is rolling.

Once $\epsilon(N)$ is determined as a function of the number of e-folds before the end of inflation N , the relation between number of e-folds and the field ϕ is determined from

$$\frac{d\phi}{dN} = \frac{M_{\text{pl}}}{2\sqrt{\pi}} \sqrt{\epsilon}, \quad (8)$$

while the Hubble parameter is established from

$$\frac{1}{H} \frac{dH}{dN} = \epsilon. \quad (9)$$

With $\epsilon(\phi)$ and $H(\phi)$ reconstructed, one can also obtain the inflaton potential through the Hamilton-Jacobi equation

$$V(\phi) = \left(\frac{3M_{\text{pl}}^2 H^2(\phi)}{8\pi} \right) \left[1 - \frac{1}{3}\epsilon(\phi) \right]. \quad (10)$$

Using equation (10) and the expressions in (1), one can write $(\ddot{a}/a) = H^2(\phi)[1 - \epsilon(\phi)]$. Inflation is defined as $(\ddot{a}/a) > 0$, which happens as long as $\epsilon(\phi) < 1$. We use this criteria in each of the numerically generated models, such that the end of inflation occurs when $\epsilon(\phi) \rightarrow 1$.

Note that there is an overall constant of H_0 here that is not set by the differential equations. This constant can be established based on the observed amplitude of either tensor or scalar fluctuations at a specific scale. Here, we will normalize our models based on the amplitude of density fluctuations at scales corresponding to CMB observations as determined by WMAP data. Since models are normalized to CMB, we pick the fiducial physical scale that corresponds to $\phi_{\text{CMB}} = 0$ to match the usual pivot point of CMB observables at $k_{\text{CMB}} = 0.002 \text{ Mpc}^{-1}$. Beyond this pivot point, the physical wavenumber is associated with a value of ϕ through

$$\frac{d\phi}{d\ln k} = -\frac{M_{\text{pl}}}{2\sqrt{\pi}} \frac{\sqrt{\epsilon}}{1 - \epsilon}. \quad (11)$$

Our convention is such that $\phi > 0$ corresponds to scales smaller than k_{CMB} ($k > 0.002 \text{ Mpc}^{-1}$) such that one is going ahead in time.

At a given wavenumber, the observable power spectra of tensor and scalar perturbations are given as [34]

$$\begin{aligned} P_T(k) &= \frac{16}{\pi} [1 - (\chi + 1)\epsilon]^2 \left(\frac{H}{M_{\text{pl}}} \right)^2 \Big|_{k=aH} \\ P_S(k) &= \frac{[1 - (2\chi + 1)\epsilon + \chi\eta]^2}{\pi\epsilon} \left(\frac{H}{M_{\text{pl}}} \right)^2 \Big|_{k=aH} \end{aligned} \quad (12)$$

when $\chi = -2 + \ln 2 + \gamma$ and $\gamma = 0.5772156649$ is the Euler-Mascheroni Constant. This allows us to set the overall normalization H_0 such that at k_{CMB} we take

$$P_S(k = 0.002) = (2.45 \pm 0.23) \times 10^{-9}, \quad (13)$$

consistent with WMAP [1]. This normalization is equivalent to setting:

$$\frac{H(\phi_{\text{CMB}}) [1 - (2\chi + 1)\epsilon(\phi_{\text{CMB}}) + \chi\eta(\phi_{\text{CMB}})]}{M_{\text{pl}} \sqrt{\pi\epsilon(\phi_{\text{CMB}})}} \approx 4.9 \times 10^{-5}, \quad (14)$$

and for most practical purposes the term within the square bracket can be ignored [36]. With our choice that CMB scale is at $\phi = 0$, in equation (5), $H_0 = H_{\text{CMB}}$.

Instead of amplitude at power-spectra at each k , the observables are generally described in terms of the power-law variables given as

$$\begin{aligned} n_S &= 1 + \sigma - (5 - 3C)\epsilon^2 - \frac{1}{4}(3 - 5C)\sigma\epsilon + \frac{1}{2}(3 - C)\xi \\ n_T &= -2\epsilon - (1 - C)\epsilon^2 + \frac{1}{2}(1 + C)\epsilon\sigma \\ \alpha_S &\equiv \frac{dn_S}{dlnk} = -\frac{1}{4} \left(\frac{1}{1 - \epsilon} \right) \\ &\times [2(C - 3)(^3\lambda_H) - 2\xi [4 + (5C - 3)\epsilon - (C - 3)\sigma] \\ &+ \epsilon[4(11 + 3C)\epsilon^2 + \epsilon[48 + (31 - 9C)\sigma] \\ &+ \sigma(20 + (3 - 5C)\sigma)]] \\ \alpha_T &\equiv \frac{dn_T}{dlnk} = \frac{1}{1 - \epsilon} \\ &\times [2(\epsilon\sigma + 2\epsilon^2)2\epsilon(1 - C)(\epsilon\sigma + 2\epsilon^2) \\ &- \frac{1}{2}(1 + C) \left(-3\epsilon^2\sigma - \frac{1}{2}\epsilon^3 + 2\epsilon(^2\lambda_H) + \epsilon\sigma^2 \right)] \end{aligned} \quad (15)$$

where $C = 4(\ln 2 + \gamma) - 5 = 0.08145$. For simplicity, we also discuss the tensor-to-scalar ratio defined at a particular scale as

$$r \equiv \frac{P_T(k)}{P_S(k)} \quad (16)$$

which in terms of slow-roll parameters is

$$r = 16\epsilon [1 - C(\sigma + 2\epsilon)]. \quad (17)$$

To the first order in slow roll parameters, $r \approx -8n_t$, which is considered to be a consistency relation that can

be used to validate inflationary models. We will discuss the accuracy to which this relation is valid at both CMB and direct detection scales. Though we can only expect a measurement of the tensor amplitude at 0.1 Hz with direct detection experiments, we will discuss the relation between tensor-to-scalar ratio at CMB scales r_{CMB} and the same ratio at direct detection frequencies, $r_{0.1\text{Hz}}$. Due to the scale dependence of the scalar and tensor tilts, these two ratios are not expected to be equal for a general inflationary potential.

To generate a family of models, we follow the usual recipes outlined in the literature [17, 21, 22]. We take the initial conditions to be sampled with in the parameter range of

$$\begin{aligned} \epsilon_0 &\in [0, 0.8] \\ \sigma_0 &\in [-0.5, 0.5] \\ \xi_0 &\in [-0.05, 0.05] \\ {}^{\ell}\lambda_{H|0} &\in [-0.025 \times 5^{-\ell+3}, 0.025 \times 5^{-\ell+3}], (3 \leq \ell \leq 10) \\ {}^{11}\lambda_{H|0} &= 0, \end{aligned}$$

such that the hierarchy is truncated at the tenth order in HSR parameters. We solve the flow equations for each set of numbers randomly drawn within the above ranges. Assuming each of the ranges is uniform, we establish $[\epsilon(N), {}^{\ell}\lambda_H(N)]$. We require that inflation last between 46 and 67 e-folds, roughly consistent with known constraints [30, 31]. With $\epsilon(N)$, we also solve for the relation between ϕ and N and between ϕ and k .

The latter establishes primordial power spectra as a function of k . The relations also establish the power-law observables at a given wave number, though to compare with observations we restrict them to the values at CMB scale, with $k_{\text{CMB}} = 0.002 \text{ Mpc}^{-1}$, and $k_{\text{dir}} = 6.47 \times 10^{13} \text{ Mpc}^{-1}$. The large number of e-folds between these two scales, $\Delta N = \ln(k_{\text{dir}}/k_{\text{CMB}}) \sim 38$, is expected to improve constraints on the inflationary model since the potential will be probed at two largely different field values [15].

Using the above initial conditions, we ran close to 20 million individual models [37]. Out of these 20 million models, roughly 20,000 models are found to fall within WMAP 95% confidence level constraints of $r_{\text{CMB}} < 0.38$ and $0.92 < n_s < 1.06$. The latter are suggested from recent cosmological data analyses (see e.g. [1], [6]) and broadly describe the allowed parameter ranges within the 2σ confidence level. In Fig. 1, we summarize the (n_s, r) plane and the distribution of model points. We will discuss these and other results in Section III.

B. Analytical Models of Slow-Roll Inflation

In addition to the numerical method to describe inflationary predictions, we also make use of several analytical models of slow-roll inflation to connect CMB observables with those at direct detection experiment levels. Unlike the previous subsection where flow equations allow us

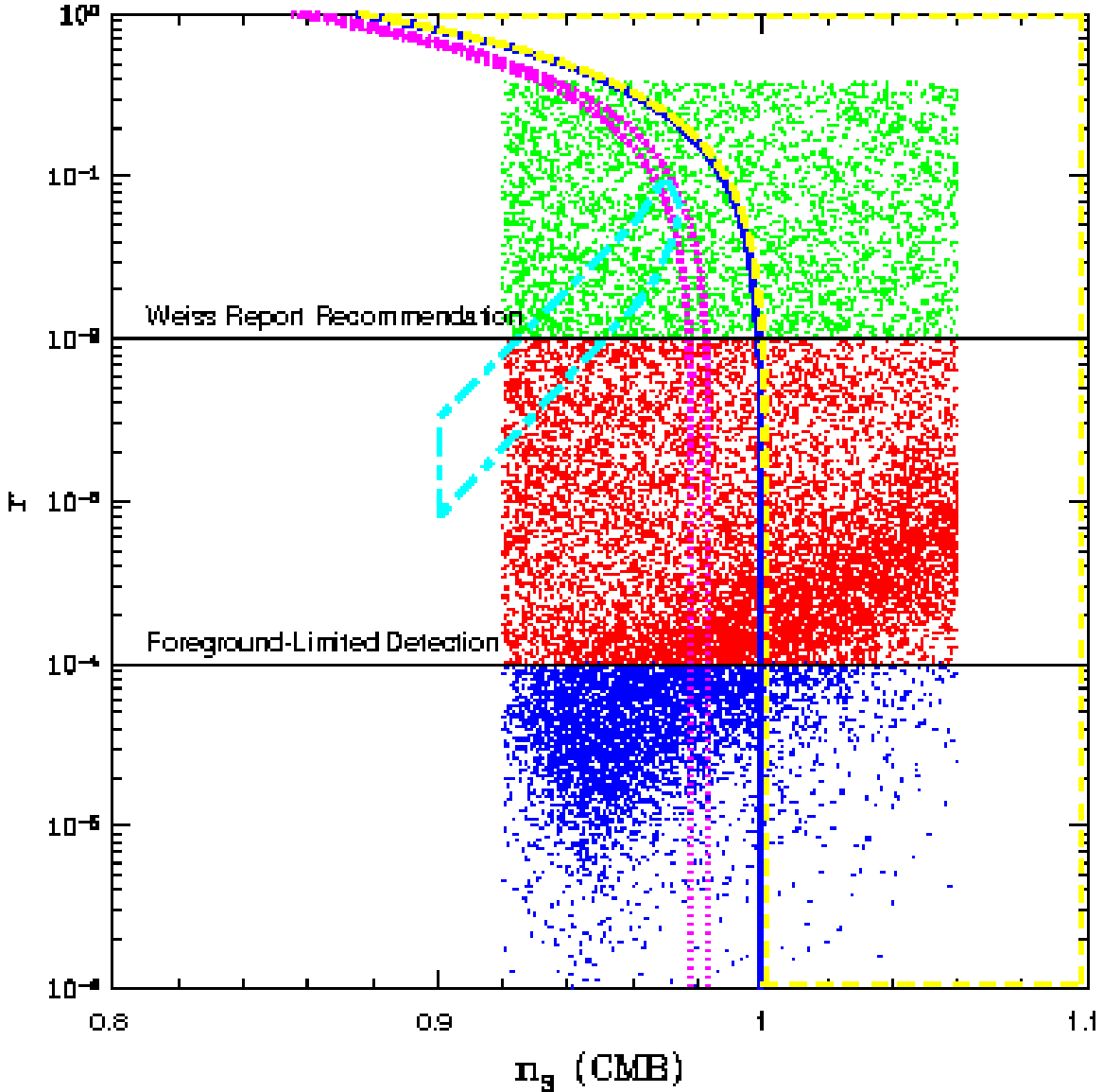


FIG. 1: The region in (n_s, r) plane consistent with WMAP CMB data at the 2σ confidence level with $r_{\text{CMB}} < 0.38$ and $0.92 < n_s < 1.06$, where r_{CMB} is the tensor-to-scalar ratio and n_s is the scalar spectral index, or tilt. Both these parameters are determined at CMB scales with $k = 0.002 \text{ Mpc}^{-1}$. Inflationary models corresponding to each model point shown here also give rise to $N > 46$ e-folds in the scale factor before the end of inflation. For comparison, we also plot the parameter space occupied by four models of inflation outlined in Section II B: power-law (solid blue line), chaotic (dotted magenta), symmetry breaking (dot-dashed cyan), and hybrid (dashed yellow) models. The two horizontal lines outline the expectation on the tensor-to-scalar ratio from CMB studies. The two values are chosen to the target goal of the next generation CMB polarization experiment ($r_{\text{CMB}} > 10^{-2}$) and an optimistic limit related to polarized foreground confusion ($r_{\text{CMB}} > 10^{-4}$). A more realistic estimate on the foreground confusion will suggest that CMB studies will be limited anywhere between a tensor-to-scalar ratio of 10^{-3} to 10^{-4} .

to describe the dynamics without specifying a particular shape for $V(\phi)$, with analytical models, we are required to specify the potential explicitly. For easy comparison, we take the same four families of models as those considered in Ref. [15]. These models describe both single field models and hybrid inflation models. The four potentials

considered here are

$$\begin{aligned}
 V(\phi) &= V_0 e^{-p\phi/M_{\text{Pl}}}, && \text{Power - law} \\
 V(\phi) &= V_0 \left(\frac{\phi}{M_{\text{Pl}}} \right)^\alpha && \text{Chaotic} \\
 V(\phi) &= V_0 \left[1 - \left(\frac{\phi}{\nu} \right)^2 \right]^2 && \text{Symmetry - breaking} \\
 V(\phi) &= V_0 \left[1 + \left(\frac{\phi}{\mu} \right)^2 \right], && \text{Hybrid}
 \end{aligned} \tag{18}$$

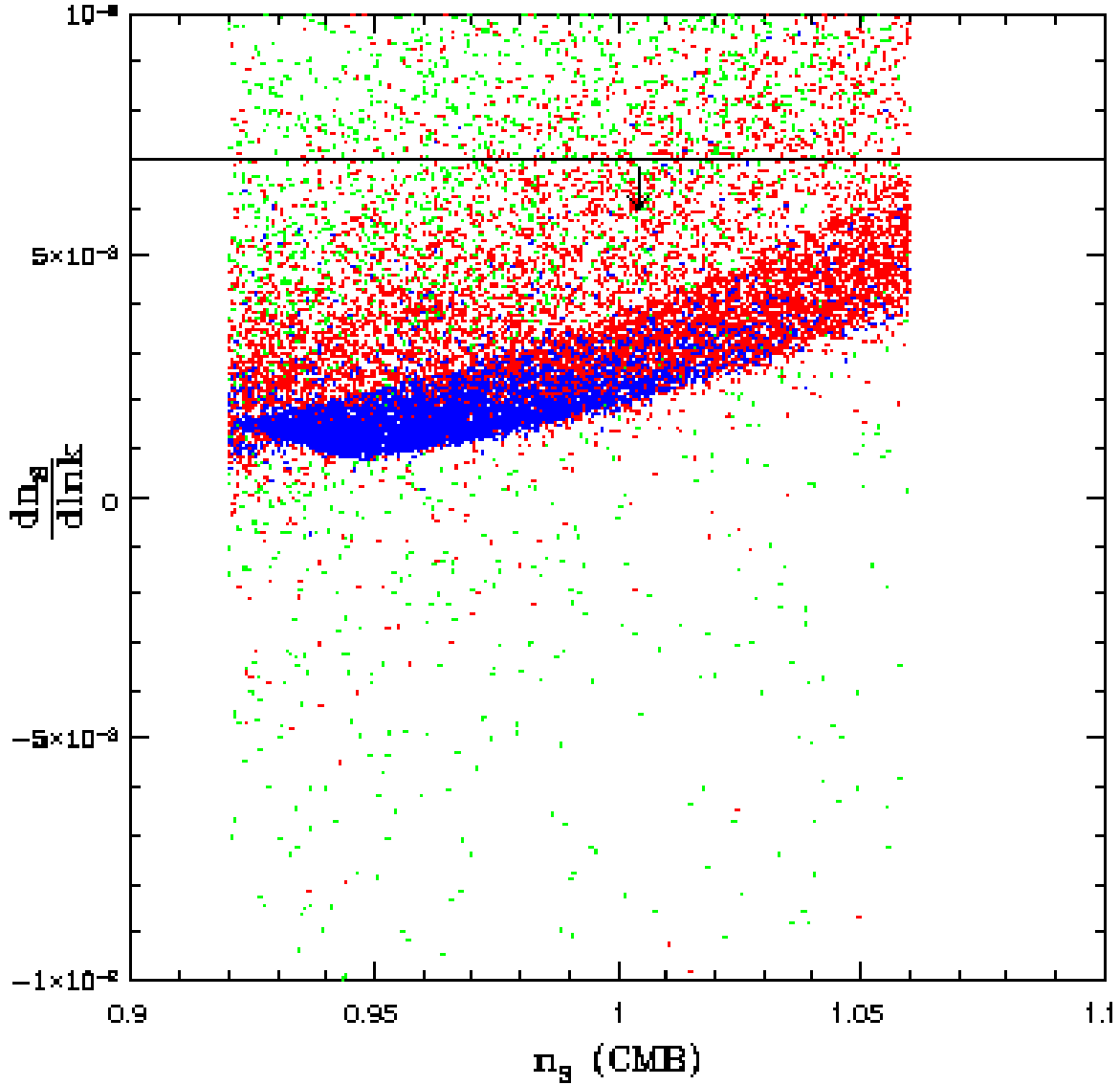


FIG. 2: The running of the scalar spectral index against the spectral index at CMB scales. We did not constrain the running, although a majority of the models fall below 10^{-2} and have positive running. The horizontal line at $\frac{dn_S}{dk} = 0.007$ shows the WMAP 2σ upper-limit on the running of the scalar spectral index.

and describe power-law, chaotic, symmetric breaking, and hybrid inflation, respectively from top to bottom. The calculation involves simply matching the observables at CMB scales (n_s, r) to free parameters in each of the potentials, such as α and ν , and also uses the number of e-folds between CMB horizon exit and the end of inflation. The amplitude of density perturbations $P_S(k_{\text{CMB}})$ fixes the overall potential normalization given by V_0 . With V_0 and free parameters fixed, and taking $\Delta N = 38$, we calculate the observables in terms of $\Omega_{\text{GW}} h^2$ (see below) and n_T and, in cases where running is not zero, α_T at the field value ϕ corresponding to direct detection experiments. We do not reproduce the analytical expressions associated with the calculation of predictions under these models as these are either readily available in Ref. [15] or

derived through equations outlined there.

C. Direct Detection Observables

While CMB measurements involve $P_S(k)$ and $P_T(k)$, direct detection measurements involve $P_T(k)$ only. As we discuss later, the lack of information on the primordial scalar spectrum at direct detection frequencies complicates simple tests and studies related to slow-roll inflation using data from direct detection experiments alone. Furthermore, since the observations involve the relic background today, one must also account for the evolution of the tensor mode from high redshifts to low redshifts. This evolution of a single gravitational wave mode can

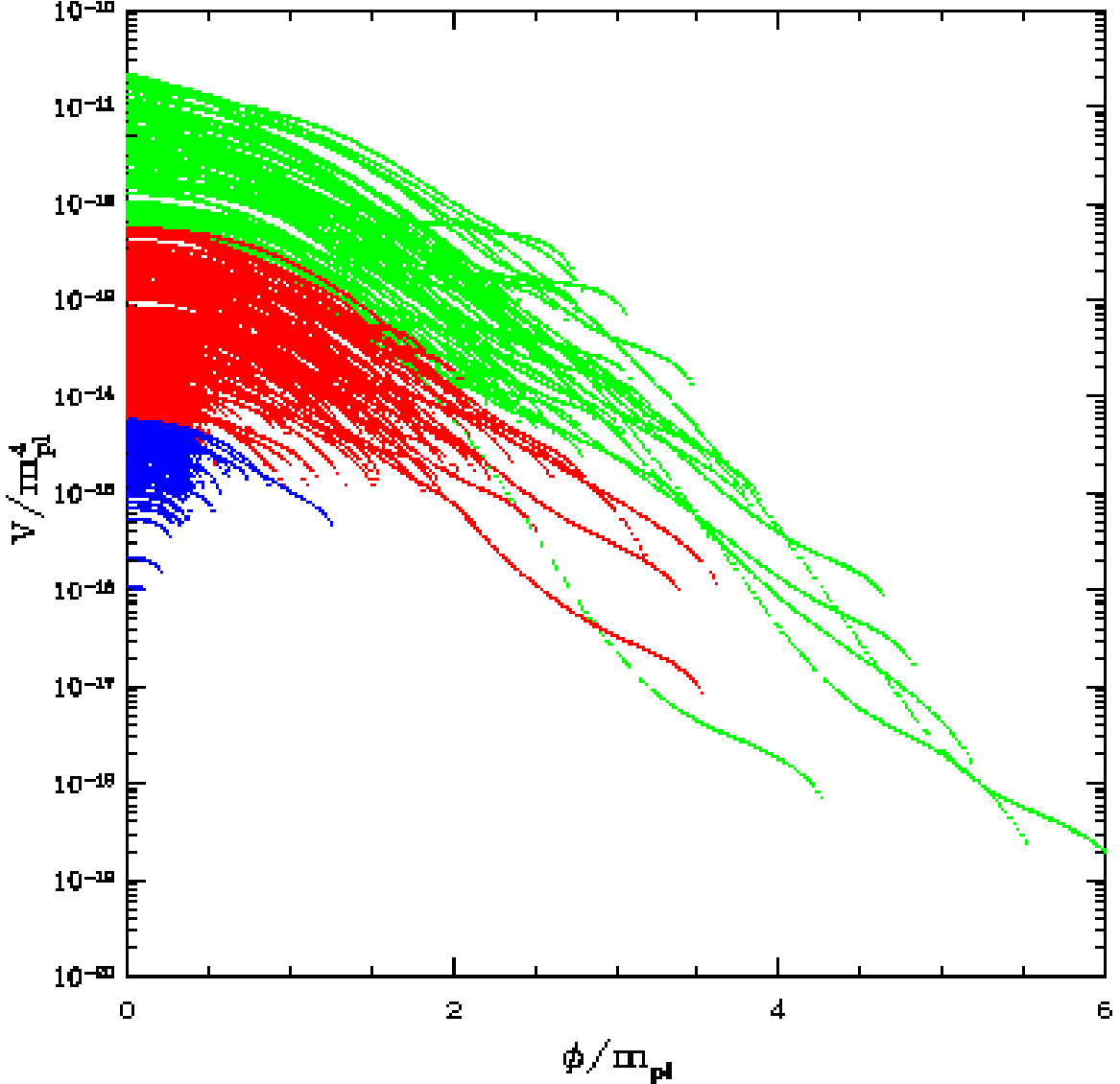


FIG. 3: The set of potentials that give rise to points shown in Figure 1 from the Monte-Carlo inflationary flow analysis. Here $\phi = 0$ corresponds to observations at CMB scales with $k = 0.002 \text{ Mpc}^{-1}$, while $\phi > 0$ corresponds to scales smaller than CMB. The potentials are subdivided based tensor-to-scalar ratio at CMB. Potentials that give rise to large tensor-to-scalar ratios with $r_{\text{CMB}} > 10^{-2}$ cannot simply be described by simple power-laws or any particular shape.

be written through the massless Klein-Gordon equation

$$\frac{d^2 h_k}{d\tau^2} + 2 \frac{1}{a} \frac{da}{d\tau} \frac{dh_k}{d\tau} + k^2 h_k = 0 \quad (19)$$

with the boundary conditions $h_k(0) = P_T(k)^{1/2}$ and $\dot{h}_k(0) = 0$. Here, τ is conformal time. We define $g_k(\tau) \equiv h_k(\tau)a(\tau)$. With this definition, we are able to rewrite the above equation,

$$\frac{d^2 g_k}{d\tau^2} + \left(k^2 - \frac{1}{a} \frac{d^2 a}{d\tau^2} \right) g_k = 0. \quad (20)$$

There are two limiting behaviors for g_k : before horizon entry $g_k \propto a \rightarrow h_k = \text{constant}$; after horizon entry g_k will oscillate which implies h_k will oscillate with an amplitude

decreasing as $1/a$ [19]. Therefore, the current spectrum of gravitational waves is determined by the primordial power spectrum and by the rate at which scales enter the horizon (i.e. the evolution of the scale factor): $h = h_0 a_k/a$. During radiation domination, $H \propto a^{-2}$, so that $k = 1/a_k$ and during matter domination $H \propto a^{-3/2}$, so that $k = 1/a_k^{1/2}$. From these relations, we find

$$h_k \propto k^{-1} \text{ (Radiation Domination)} \quad (21)$$

$$h_k \propto k^{-2} \text{ (Matter Domination).} \quad (22)$$

These scalings are generally quantified in terms of the transfer function $T_T(k)$ for tensor modes [19], such that the tensor power spectrum is related to the one generated

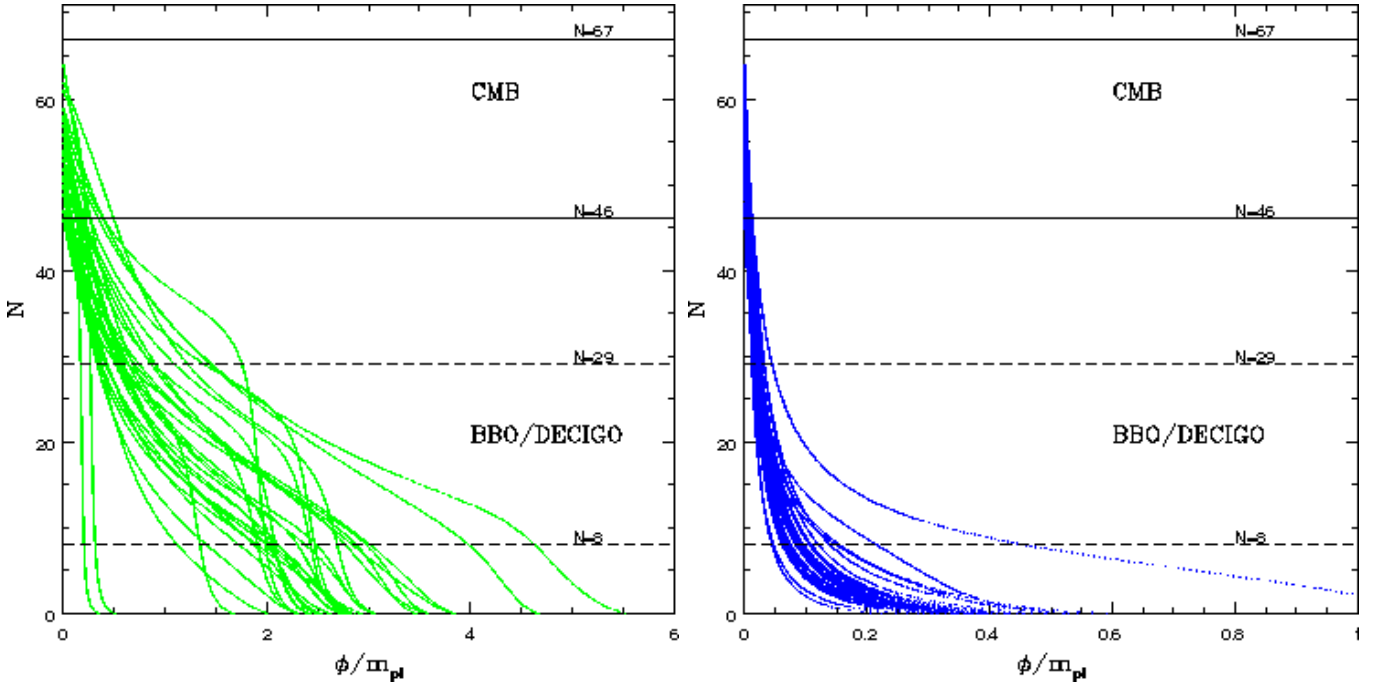


FIG. 4: The relation between the number of e-folds N and ϕ , the value of the inflaton field, for representative sampling of potentials shown in Figure 3. In the left panel, we make use of potentials that give rise to $r_{\text{CMB}} > 10^{-2}$, while in the right panel, we concentrate on the relation between N and ϕ for potentials that lead to $r_{\text{CMB}} < 10^{-4}$. In the case of potentials that lead to large r_{CMB} , $V(\phi)$'s are shaped such that there is a significant, and an abrupt, increase in the number of e-folds over a small variation in ϕ . The ϕ values related to this abrupt changes in N correspond to the field values where the inflaton potentials in Figure 3 flatten. On the other hand, N versus ϕ relations for potentials that results in a small r_{CMB} are gradual. A behavior similar to this was already described in Ref. [17] based on the relation between $H(N)$ versus N such that models that lead to large tensor amplitude have abrupt changes in $H(N)$. The horizontal lines indicate the number of e-foldings related to CMB (top two lines) and direct detection (bottom two lines) observations.

during inflation as

$$P_T(k, t = t_0) = P_T(k, t = t_\infty) T_T^2(k). \quad (23)$$

We define the ratio of energy density of the gravitational wave background to the critical closure density as

$$\Omega_{\text{GW}}(k) = \frac{1}{\rho_c} \frac{d\rho_{\text{GW}}}{d \ln k}. \quad (24)$$

and write

$$\Omega_{\text{GW}}(k) h^2 = \frac{c^2 k^2 h^2}{6H_0^2} \langle |h_k|^2 \rangle \equiv A_{\text{GW}} P_T(k), \quad (25)$$

where $A_{\text{GW}} = 2.74 \times 10^{-6}$ at $f = 0.1$ Hz [15] and comes from taking a frequency average of the tensor transfer function $T_T(k)$. The mapping amplitude A_{GW} ignores the anisotropic stresses in the cosmic fluid, among which free-streaming of relic neutrinos is important [29]. The additional damping of tensor modes, however, is only restricted to modes that enter the horizon after neutrino free-streaming or the gravitational wave background at frequencies below 10^{-11} Hz. Thus, our calculations are not affected by ignoring anisotropic stresses. We do note that other exotic processes may damp gravitational waves

at frequencies of 0.1 Hz [28], but the physical processes are mostly speculative and we do not consider them to be important for this calculation.

In addition to the amplitude of the gravitational wave background captured by $\Omega_{\text{GW}} h^2$, recent analyses suggest that it may also be possible to measure the tilt n_T of the gravitational wave background at direct detection frequencies [26]. Thus, we discuss the observables in terms of both $\Omega_{\text{GW}} h^2$ and n_T here. For direct detection experiments, we consider three possibilities here involving BBO and an improved version of BBO (BBO-grand) as well as DECIGO. These experiments and their sensitivities are summarized in Ref. [26], and to be consistent with those calculations, we make use of the same quoted sensitivities here. We do not consider a version of BBO called BBO-lite with a sensitivity to gravitational waves only down to $\Omega_{\text{GW}} h^2$ of 10^{-15} . As we find later, such an experiment is unlikely to result in any detection of the gravitational wave background as current limits already rule out a background just above this level.

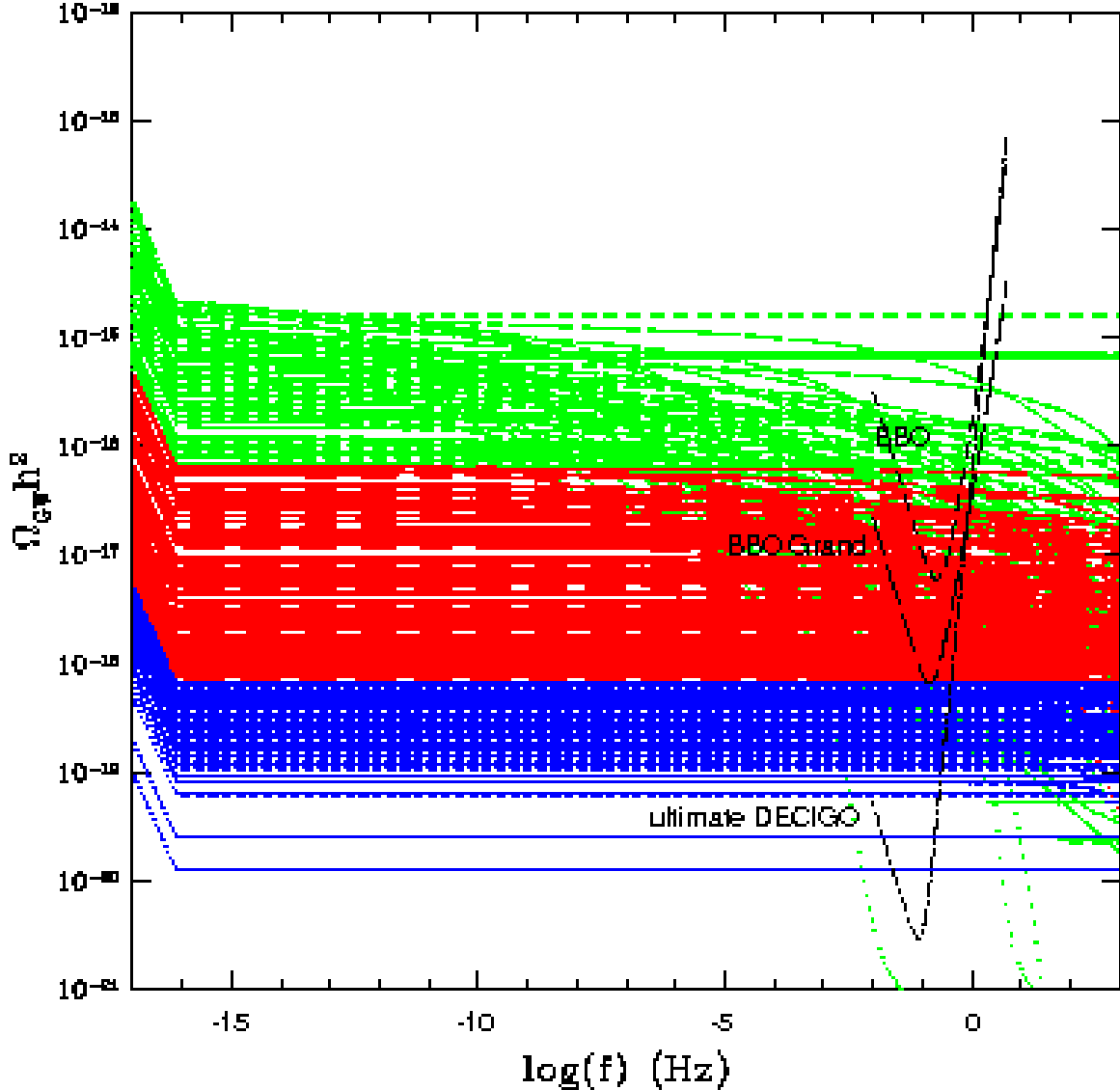


FIG. 5: The amplitude of the stochastic gravitational wave background, $\Omega_{\text{Gw}} h^2$, versus the gravitational wave frequency. The curves, subdivided by the tensor-to-scalar ratio at CMB scales, represent the expectations based on inflationary models selected from solving inflationary flow equations and consistent with WMAP+SDSS data. The models that lead to large tensor-to-scalar ratios generally have large spectral indices for the gravitational wave background resulting in a damping of the power at frequencies related to direct detection experiments. We also show the detector sensitivities for a 5 year-long integration of some of the options discussed in the literature. These experiments, from top to bottom, are BBO, an improved version of BBO (BBO-Grand), and an extremely optimistic version of the DECIGO (Ultimate DECIGO).

III. RESULTS

A. CMB Predictions and Comparison

Figure 1 summarizes the plane of tensor-to-scalar ratio versus scalar tilt at CMB scales ($k = 0.002 \text{ Mpc}^{-1}$), where points represent results of the Monte-Carlo process using the flow equations. We constrain the parameter space to be $r_{\text{CMB}} < 0.38$ and $0.92 < n_s < 1.06$ at the 95% confidence level following the results of Ref. [1] and Ref. [6].

In addition to lying within this range, we also require that each of the selected models generates between 46 and 67 e-folds before the end of inflation. The two horizontal lines represent the expected limits from CMB observations: the published goal of the next generation NASA CMB polarization mission with a tensor-to-scalar ratio of 10^{-2} [7] and an optimistic limit on the tensor-to-scalar ratio based on polarized foregrounds (10^{-4}). This limit is somewhat unknown and estimates suggest that it is between 10^{-3} and 10^{-4} [8], depending on the frequency selection, the sky area targeted for CMB observations, and the unknown polarized intensity of dust. Once high

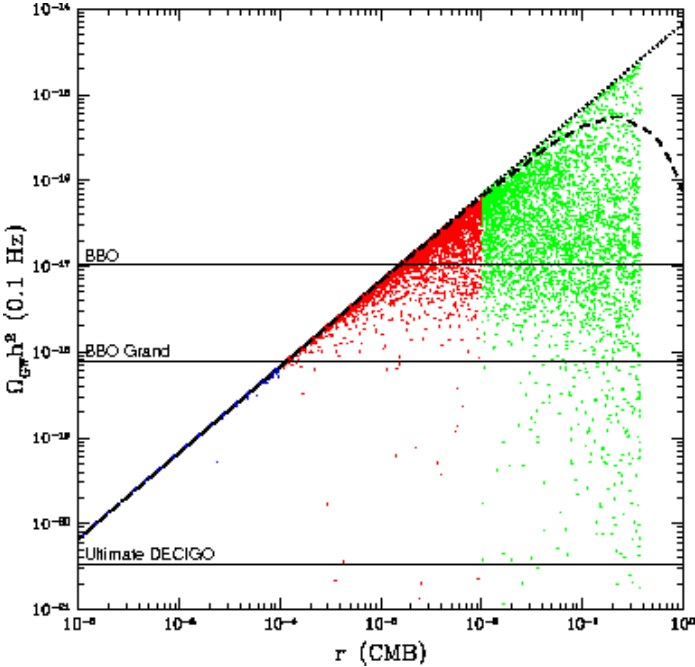


FIG. 6: The amplitude of the gravitational wave background at 0.1 Hz $\Omega_{\text{GW}} h^2$ plotted in terms of the tensor-to-scalar ratio at CMB scales ($k = 0.002 \text{ Mpc}^{-1}$). For reference, we also show the minimum background amplitude that can be detected with a signal-to-noise ratio of unity with BBO, BBO-Grand, and Ultimate DECIGO. The relation between $\Omega_{\text{GW}} h^2$ and r_{CMB} is such that one can establish an upper limit on the expected amplitude of the gravitational wave background at a given tensor-to-scalar ratio. The dotted line shows the relation, which we discuss in equation 27. An experiment such as BBO-Grand can probe slow-roll inflationary models with tensor-to-scalar ratio greater than 10^{-4} .

frequency all-sky CMB polarization maps become available with Planck, this foreground-limited tensor-to-scalar ratio will be better established. To guide our discussion, here, we take the lower limit of 10^{-4} .

In addition to inflationary flow equation predictions, we also show the expected range allowed by the model parameter space of several families of analytical models of inflation. These include the power-law, chaotic, symmetry breaking, and Hybrid inflation models. The allowed ranges we highlight here are consistent with previous calculations [15] and both analytical and Monte-Carlo numerical models are normalized to the same amplitude of the scalar perturbations at $k = 0.002 \text{ Mpc}^{-1}$. As is well known, hybrid inflation models generally allow $n_s > 1$, while other families generally fill up the parameter space with $n_s < 1$.

For comparison, in Figure 2, we plot the scalar spectral index against the running of the scalar spectral index, α_s , at CMB scales. The top line indicating an arrow pointed to low values of α_s is roughly the upper limit on the running of scalar tilt with a value of 0.007 at the 95% confidence level using WMAP+SDSS data [6]. At the

low end, the running is allowed to be as low as -0.13 and all our data points lie above this limit. While some of our models lie above $\alpha_s = 0.007$, we do not impose a selection based on α_s , as we have seen from the literature that the determination of α_s is largely subject to assumptions coming from model fitting. As an example, in Ref. [32], α_s is constrained to be below 0.01 at the 1σ confidence level with a prior of 30 e-folds or more between CMB and the end of inflation.

The corresponding potentials allowed by the inflationary flow analysis in the (n_s, r_{CMB}) plane are shown in Figure 3. The potentials are subdivided based on the tensor-to-scalar ratio at CMB scales. In Figure 3 $\phi = 0$ corresponds to CMB scales while $\phi > 0$ represents scales below CMB. The potentials are truncated at the end of inflation when ϵ reaches a value of unity, and again, all these potentials lead to between 46 and 67 e-folds of inflation. As shown, potentials that give rise to large tensor-to-scalar ratios with $r_{\text{CMB}} > 10^{-2}$ cannot be described by simple power-laws or with any particular analytical shape. In fact, almost all of the potentials cannot be described by simple analytical forms.

In general, inflationary potentials with $r_{\text{CMB}} > 10^{-2}$ have $\Delta\phi > M_{\text{pl}}$, where $\Delta\phi$ corresponds to the number of e-folds from CMB horizon exit to end of inflation. This result is well known in terms of the Lyth-bound [33]. In Fig. 4, we summarize the relation between the number of e-folds N and the field value ϕ for potentials that give rise to $r_{\text{CMB}} > 10^{-2}$ (left panel) and $r_{\text{CMB}} < 10^{-4}$ (right panel). As can be seen in Fig. 3, potentials that lead to large tensor-to-scalar ratio at CMB scales have structure such that towards the end of inflation potentials begin to flatten followed by a drop in the amplitude as $\epsilon \rightarrow 1$. Since the number of e-folds between two field values can be written as

$$N(\Delta\phi) \approx \frac{8\pi}{M_{\text{pl}}^2} \int_{\phi_i}^{\phi_f} \frac{V(\phi)}{V'(\phi)} d\phi, \quad (26)$$

and since $V'(\phi)$ becomes smaller towards the end of inflation, one finds a large change in the number of e-folds. In Fig. 4 we show some example relations between N and ϕ which highlight the fact that most potentials that lead to $r_{\text{CMB}} > 10^{-2}$ behave such that the last 20 to 30 e-folds of inflation happen suddenly over a small duration of $\Delta\phi$. The models with steep slopes around $\phi = 2$ are prime examples of this behavior. Similar potential shapes have been noted before and explained in terms of the relation between $H(N)$ and N in Ref.[17]. As discussed there, direct detection experiments that are only sensitive to gravitational wave backgrounds with large r_{CMB} values will be probing potentials with this abrupt behavior. None of the analytical models have behaviors like this. In addition to the changes in the number of e-folds, the shapes of these potentials are such that, as we discuss in the next subsection, the tensor tilt is strongly scale dependent. Because of the negative value of the scale dependent tensor tilt, the gravitational wave background amplitude at direct detection scales becomes lower than

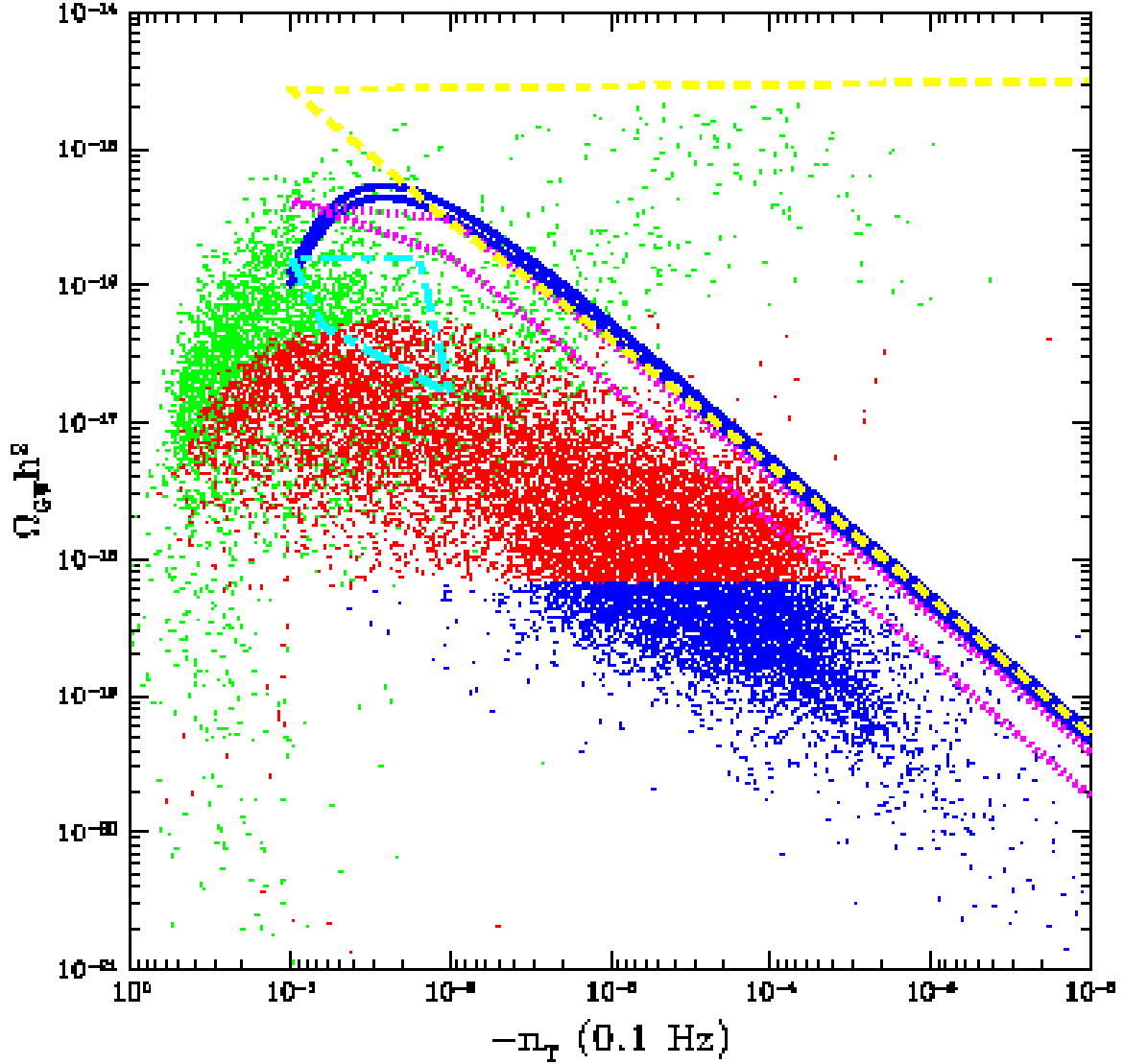


FIG. 7: The amplitude of the gravitational wave background $\Omega_{\text{GW}} h^2$ at 0.1 Hz plotted against the spectral index of the gravitational wave background power spectrum at 0.1 Hz. We determine this spectral index using the inflationary flow equations with $n_T(\phi)$ determined at the scalar field value ϕ corresponding to 0.1 Hz. In solid, dotted, dot-dashed and dashed curves, we show regimes in the $\Omega_{\text{GW}} h^2 - n_T$ plane at 0.1 Hz populated by power-law, chaotic, symmetry breaking, and hybrid models of inflation. In contrast to Figure 1, where there is a large overlap between Monte-Carlo models and analytical models at $k = 0.002 \text{ Mpc}^{-1}$, we find that the predictions based on inflationary flow equations depart significantly from predictions of the analytical models at $k \sim 6.5 \times 10^{13}$.

the case where tensor tilt is scale independent.

B. Predictions for Gravitational Wave Observations

With observables at CMB scale defined and models selected based on the WMAP+SDSS constraints, we now extend the discussion to consider the predictions for gravitational wave detection at direct detection frequencies. Figure 5 shows the prediction for $\Omega_{\text{GW}} h^2$ as a function of frequency, where in addition to the power spectrum of tensor perturbations generated during inflation, we also

take into account the evolution through the transfer function (See, Section II C). As can be seen in Figure 5, the potentials that have large variations lead to significant spectral indices for the tensor power spectrum, while for $r_{\text{CMB}} < 10^{-4}$ the tensor tilt is insignificant and the approximation that $n_T \approx 0$ is reasonably accurate. The correspondence between large r_{CMB} and large n_T impacts planning of direct detection experiments. For reference, in Figure 5, we also plot the sensitivity curves of three of the experimental options that are routinely discussed in the literature [15, 16, 17, 18]. The sensitivity curves are the same ones shown in Ref. [26] which were used to estimate how well these interferometers can study the

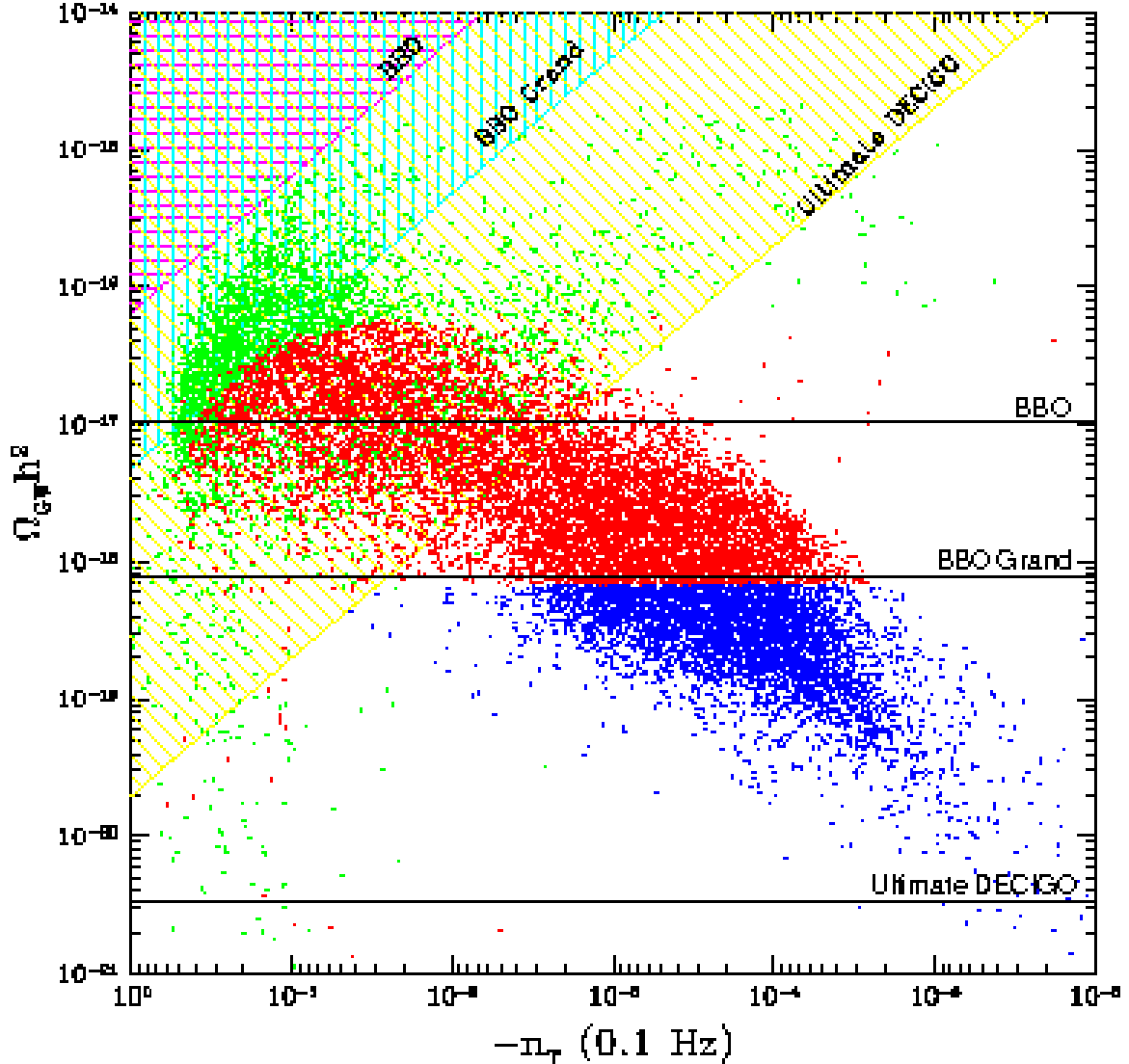


FIG. 8: The amplitude of the gravitational wave background at 0.1 Hz plotted in terms of the spectral index of the gravitational wave background power spectrum at 0.1 Hz. The data points are same as those in the previous figure. Here, we put the measurements in the context of experimental studies. The horizontal lines show the minimum amplitude of the gravitational wave background detectable with a signal-to-noise ratio of one. The shaded areas represent the regions in the $\Omega_{\text{GW}} h^2 - n_T$ plane such that these detectors can detect both the amplitude and the tensor spectral index n_T at 1σ confidence level.

gravitational wave background amplitude and the spectral index.

Figure 6 shows the relation between the amplitude of the gravitational wave background at a frequency of 0.1 Hz and the tensor-to-scalar ratio at CMB ($k = 0.002 \text{ Mpc}^{-1}$). Such a relation has been previously discussed in Refs. [16, 17]. The data points are distributed such that one clearly notices an upper limit on $\Omega_{\text{GW}} h^2$ at a fixed r , which we determine to be

$$\Omega_{\text{GW}} h^2 < 6.72 \times 10^{-15} r \left(\frac{P_s(k_{\text{CMB}})}{2.45 \times 10^{-9}} \right) \left(\frac{A_{\text{GW}}}{2.74 \times 10^{-6}} \right). \quad (27)$$

This limit agrees with the result of Ref. [17] when converting our scalar power spectrum normalization and the

transfer function to their values. This upper limit comes from the fact that under slow-roll inflation, n_T has a negative value if it is not zero. In Fig. 6, for comparison, we also produce the prediction under the power-law potential for inflation. At low values of the tensor-to-scalar ratio at CMB, there is a tight correlation between $\Omega_{\text{GW}} h^2$ and r_{CMB} , which falls along the power-law expectation.

With $r_{\text{CMB}} < 0.38$ at the 95% confidence level from current observations, the derived upper limit on the gravitational wave background at 0.1 Hz, under standard slow-roll inflation, is such that $\Omega_{\text{GW}} h^2 < 2.55 \times 10^{-15}$. Experimental options, such as the BBO-lite [26], with a limiting sensitivity of 10^{-15} in $\Omega_{\text{GW}} h^2$, are clearly unfavored as they will only explore an extremely small param-

eter space. Moreover, CMB experiments such as *Planck* will soon explore the tensor-to-scalar ratio down to a limit of 0.1, while the next generation CMB polarization mission targets to improve this down to a limit of 0.01. In terms of the amplitude alone, a direct detection experiment must have sensitivity below 6×10^{-17} in Ω_{GWh}^2 to be both useful in terms of model selection and studies related to inflation. Furthermore, even if CMB experiments were to detect a primordial tensor component with a tensor-to-scalar ratio above 0.01, an experimental option such as the standard-BBO [26] is not preferred as many of our inflationary models are such that with increasing r_{CMB} , n_T (which is negative) also increases in magnitude. This results in a large suppression of power at direct detection frequencies as shown in Fig. 5 for Ω_{GWh}^2 versus frequency for curves with $r > 0.01$.

The preference to select a direct detection experiment with adequate sensitivity down to a CMB tensor-to-scalar ratio of 10^{-4} is simply a criteria based on slow-roll inflationary models. It could be that, under non-standard hypotheses, one can generate blue-tilted models for tensor fluctuations such that one generates a large gravitational wave background at frequencies around 0.1 Hz. We refer the reader to Ref. [17] for a discussion of such possibilities. We, however, find less motivation to design a target for a direct detection experiment based on non-standard criteria alone since existing cosmological data rules out most of these cases.

C. Experimental Detection

Figures 7 and 8 highlight the gravitational wave amplitude, in Ω_{GWh}^2 as a function of the tensor tilt at a frequency of 0.1 Hz. In addition to the Monte-Carlo models generated from the inflationary flow equations, we also show the model predictions obtained from analytical models. These calculations reproduce results in Ref. [15]. Figure 8 plots the same information as in Figure 7, except that in this plot we have put the model distribution in the context of observational measurements. The horizontal lines in Figure 8 show the amplitude of the gravitational wave background that lead to a signal-to-noise ratio (SNR) of one with each of these experiments. In terms of the amplitude, BBO, BBO-grand and Ultimate DECIGO are expected to detect gravitational wave backgrounds with amplitudes $\Omega_{\text{GWh}}^2 = X \times 10^{-18}$ where $X = 10, 1, 0.01$ respectively, consistent with previous discussions regarding these experiments [16, 26].

In addition to the amplitude of the gravitational wave background, it is also useful to consider the possibility that these detectors can be used for a reliable measurement of the tensor spectral index. Following the Fisher matrix calculations in Ref. [26], we determine that for a one-sigma detection of the tensor spectral index in addition to the gravitational wave background amplitude, it is required that one roughly satisfies the relation $|n_t|(\Omega_{\text{GWh}}^2/6 \times 10^{-18}) = X$. As shown by the shaded

regions in Figure 8, the requirement that laser interferometers detect both the amplitude of the gravitational wave background and the tensor spectral index leads to a significant reduction in the model parameter space probed by these detectors. Models that have both large Ω_{GWh}^2 and n_T may be studied reliably. But even experiments such as DECIGO will not be able to detect values of $|n_T|$ less than 10^{-3} despite their ability to detect the gravitational wave amplitudes for nearly all Monte-Carlo models.

D. Testing Inflation: CMB vs. Direct Detection

While the above discussion considered the extent to which the gravitational wave background can be measured with planned interferometers such as BBO and DECIGO, we now address how CMB information can be put to use in determining the prospects for direct detection measurements. This is motivated by the fact that ongoing and upcoming CMB polarization measurements will improve the existing constraints from WMAP on the CMB tensor-to-scalar ratio and the scalar tilt and running of the scalar tilt. With predictions from CMB data, one can also optimize the sensitivity requirements for a detection of the gravitational wave background. Here, we address the extent to which CMB observations can be extended to study the gravitational wave background at a scale 16 orders of magnitude larger than CMB scale.

As a first approximation, one can make use of a simple power-law extrapolation to establish the expected gravitational wave background at direct detection frequencies [14]. To test the accuracy of such an extrapolation, we compare the predictions using exact numerical flow equations with the predictions calculated using a simple power-law extension between CMB and direct detection scales. For this comparison, we first write approximate forms for the scalar and tensor power spectra as

$$P_S(k) \approx P_S(k_{\text{CMB}}) \times \left(\frac{k}{k_{\text{CMB}}}\right)^{n_S(k_{\text{CMB}})-1+\frac{1}{2}\alpha_S(k_{\text{CMB}})\ln\left(\frac{k}{k_{\text{CMB}}}\right)}$$

$$P_T(k) \approx P_T(k_{\text{CMB}}) \left(\frac{k}{k_{\text{CMB}}}\right)^{n_T(k_{\text{CMB}})-1+\frac{1}{2}\alpha_T(k_{\text{CMB}})} \quad (28)$$

We can write the gravitational wave background at direct detection frequencies as

$$\Omega_{\text{GWh}}^2 = A_{\text{GW}} P_T(k=0.1\text{Hz})$$

$$P_T(k=0.1\text{Hz}) = r_{0.1\text{Hz}} P_S(k=0.1\text{Hz}). \quad (29)$$

We assume that the tensor background satisfies the slow-roll consistency relation of $n_T = -r/8$ and that the tensor power spectrum is not running with $\alpha_T = 0$. This allows us to write an approximate equation for the tensor-

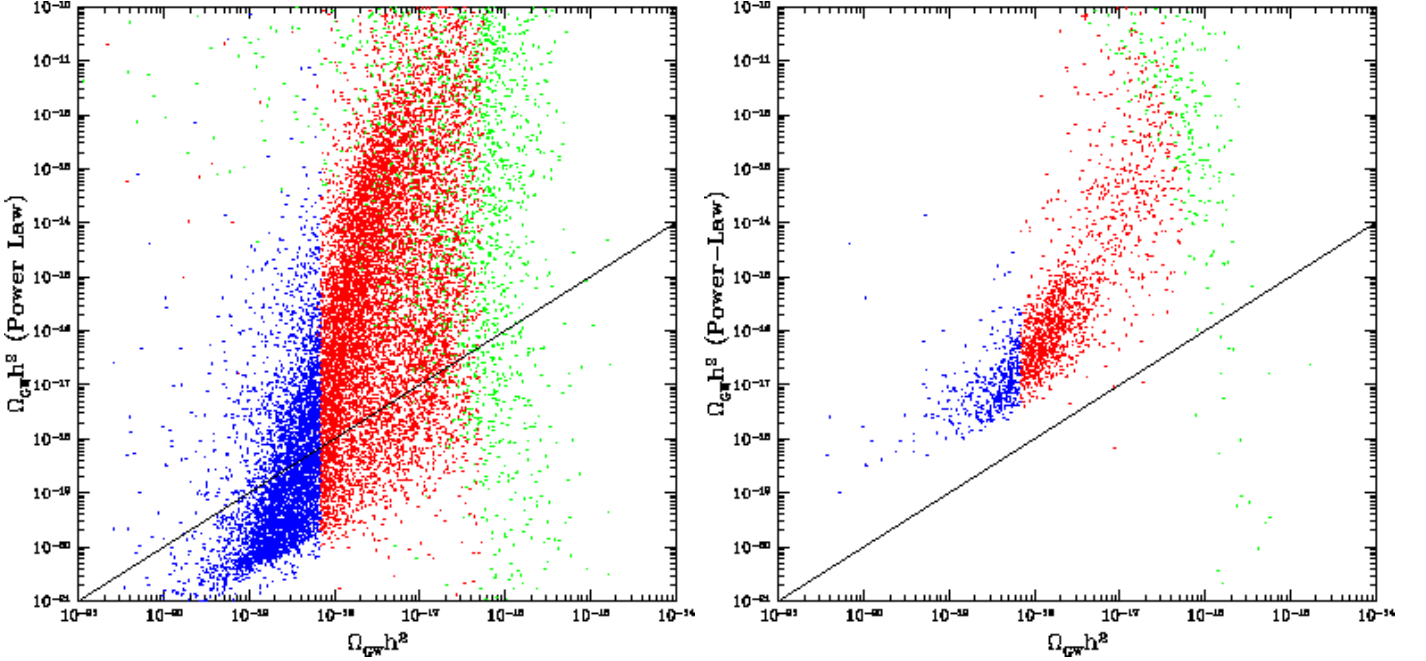


FIG. 9: $\Omega_{\text{GW}}h^2$ at 0.1 Hz plotted against the estimated $\Omega_{\text{GW}}h^2$ assuming a power-law expansion. The solid line at an angle represents the case where $\Omega_{\text{GW}}h^2 = [\Omega_{\text{GW}}h^2]_{\text{power-law}}$. The left panel shows the relation for all data points, while the right panel selects points with $0.99 < n_s < 1.01$ at CMB scales. The power-law approximation is based on an extrapolation of CMB observations using the values r_{CMB} , $n_s(k_{\text{CMB}})$, $\alpha_s(k_{\text{CMB}})$, and the assumption that $n_T = -r_{\text{CMB}}/8$ and $\alpha_T = 0$ at all scales. This fails to capture the amplitude of the background predicted in our exact numerical calculation. The power-law approximation leads to a general overestimate of the gravitational-wave background at direct detection frequencies. While some of the scatter in the left panel is due to the large range of n_s , by selecting inflationary models with a small range in n_s , we show that the overestimate is not restricted to either large or small n_s models at CMB scales.

to-scalar ratio at direct detection scales as

$$r_{0.1\text{Hz}} \approx r_{\text{CMB}}$$

$$\times \left(\frac{k}{k_{\text{CMB}}} \right)^{n_s(k_{\text{CMB}}) - 1 + \frac{1}{2}\alpha_s(k_{\text{CMB}}) \ln\left(\frac{k}{k_{\text{CMB}}}\right) + r(k_{\text{CMB}})/8} \quad (31)$$

Using this relation and the approximate scalar power-spectrum with $n_s(k_{\text{CMB}})$ and $\alpha_s(k_{\text{CMB}})$ in equation (28), one can approximate the gravitational wave background amplitude, $[\Omega_{\text{GW}}h^2]_{\text{power-law}}$ at 0.1 Hz. In Fig. 9, we show the comparison between $[\Omega_{\text{GW}}h^2]_{\text{power-law}}$ and the exact amplitude of the gravitational wave background, $\Omega_{\text{GW}}h^2$, as calculated through numerical solutions to the flow equations. Relative to the exact $\Omega_{\text{GW}}h^2$ values that are generally below 10^{-15} , $[\Omega_{\text{GW}}h^2]_{\text{power-law}}$ ranges as high as 10^{-10} and over-predicts the gravitational wave background at direct detection frequencies. The differences are mostly significant for models that involve large CMB tensor-to-scalar ratios. These models have a small, but non-negligible, scale dependence in the tensor tilt.

Note that $n_T = -r/8$ and $\alpha_T = 0$ are simple assumptions that do not hold for general inflationary models, except in the case of power-law inflation [15]. These two assumptions also hold well for hybrid models. They do not hold, however, for chaotic and symmetry-breaking potentials as they often produce significant tensor run-

ning (see Figure 12). The predictions under the Monte-Carlo slow-roll inflation models depart significantly from analytical models where α_T is mostly zero at direct detection scales. This departure is also related to the reason why the gravitational wave background amplitude cannot be predicted by extrapolating CMB information to a scale roughly 16 orders of magnitude higher as shown in Figure 9. As highlighted in Figure 7, with non-zero α_T , chaotic and symmetry-breaking models come closest in approximating the slow-roll numerical predictions at 0.1 Hz, though the agreement is still small. Compared to all these analytical models, numerical models lead to a substantial scale dependence in the tensor tilt.

This disagreement is a concern for a simple comparison between CMB observations and direct detection experiments. At CMB scales, the observations are limited to r_{CMB} , $n_s(k_{\text{CMB}})$ and $\alpha_s(k_{\text{CMB}})$. A direct detection experiment will measure $\Omega_{\text{GW}}h^2$ and $n_T(0.1\text{Hz})$. This limited information cannot establish a unique inflationary potential. Suggestions have been made that the amplitude of tensor components can be used to establish the slope of the inflaton potential $V(\phi)$ between CMB and direct detection scales. While this is, in principle, possible, the constraints will not be unique unless a particular class of analytical inflationary models is advocated. Under the general scenario, where $V(\phi)$ can vary such that

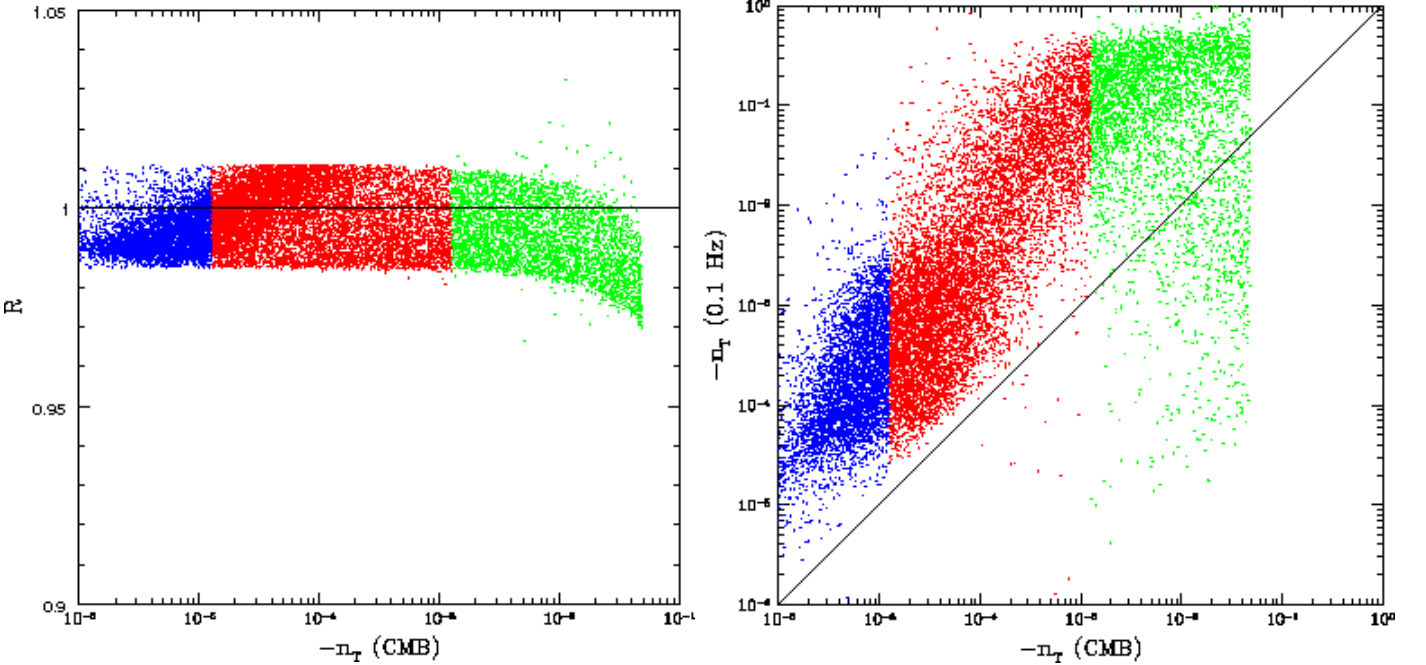


FIG. 10: *Left:* The consistency relation between the tensor amplitude r and the tensor tilt n_T . Under first order slow roll expansion, $r = -8n_T$. Here, we plot $R \equiv r/(-8n_T)$ as a function of n_T for measurements at CMB scales. This consistency relation is challenging to measure with CMB data alone due to lack of information in the CMB power spectrum for a reliable measurement of n_T . The spread in R and the tendency for R to dip slightly below one for large n_T is a result of the second order terms used to calculate r and n_T . For $-n_T > 0.01$, one sees a departure from $R = 1$ due to the fact that for these models, $n_T > -2\epsilon$ and the ϵ^2 term is more significant for n_T than for r . *Right:* In a recent study, Smith et al., it was suggested that the inflationary consistency relation can be tested by combining CMB observations with direct detection measurements under the assumption that $n_T(k_{\text{CMB}}) \approx n_T(0.1\text{Hz})$. Here, we plot the tensor spectral index at 0.1 Hz versus the same spectral index at CMB showing that n_T at 0.1 Hz is larger than the value at CMB scales and the assumption that $n_T(k_{\text{CMB}}) \approx n_T(0.1\text{Hz})$ is not consistent with the models predicted under slow-roll inflationary flow equations. In general, using direct detection slope to approximate tensor tilt at CMB scales results in a bias of an order of magnitude or more. We explain this difference in terms of the scale dependence of the tensor tilt and higher order corrections such as α_T .

the spectral indices are scale dependent, one cannot simply connect CMB scales with direct detection frequencies through a power-law extrapolation.

This complication arises due to the large difference in the two scales. This difference also complicates simple tests on slow-roll inflation. As an example, we revisit the proposed test in Smith et al. [16] on the consistency relation of $r = -8n_T$, where they assumed $n_T(k_{\text{CMB}}) \approx n_T(k = 0.1\text{Hz})$. They made this assumption because CMB observations are unlikely to measure the tensor tilt with adequate accuracy due to confusion with lensing B-modes, while direct detection experiments, especially with adequate sensitivity, can make a measurement of n_T . Using the assumption that $n_T(k_{\text{CMB}}) \approx n_T(k = 0.1\text{Hz})$ combined with the tensor-to-scalar ratio at CMB scales, Smith et al. advocated a way to test the consistency relation of the form $r_{\text{CMB}} = -8n_T(k = 0.1\text{Hz})$, though resulting constraints for experiments under consideration were not that impressive. For example, the combination of Ultimate-DECIGO and *Inflation Probe*, at best, would constrain this relation to a level of 20% if the tensor-to-scalar ratio is between 0.01 and 0.1. The

test of the consistency relation is affected by the fact that, relative to the fractional error on r at any wavenumber, one must measure n_T with a fractional error that is 8 times better.

Beyond these measurement issues, there are also fundamental problems from the theory side. To study the extent to which the assumption that $n_T(k_{\text{CMB}}) \approx n_T(k = 0.1\text{Hz})$ is accurate, in Fig. 10 (right panel), we plot $n_T(k = 0.1\text{Hz})$ versus $n_T(k_{\text{CMB}})$. As shown, there is a large difference between the two tilts such that $|n_T(k = 0.1\text{Hz})| > |n_T(k_{\text{CMB}})|$. The consistency relation will be violated if one blindly substitutes $n_T(k_{\text{CMB}}) \approx n_T(k = 0.1\text{Hz})$ (see, Figure 11), though as shown in the left-panel of Figure 10, our predictions are accurate to 1% level of the consistency relation at CMB with r_{CMB} and $n_T(k_{\text{CMB}})$.

To show one aspect from which the complications arise, in Fig. 12, we plot the tensor tilt at 0.1 Hz as a function of the running of the tensor tilt α_T , again at 0.1 Hz. For comparison, we also plot model predictions for the running of the tilt through analytical models, where some models, such as the power-law potential, are such that

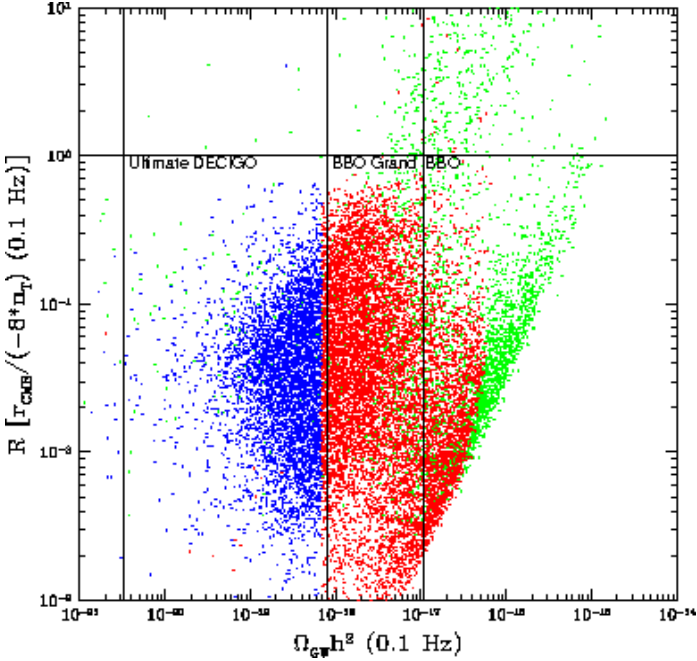


FIG. 11: The consistency relation between the tensor amplitude r and the tensor tilt n_T , $R \equiv -r/8n_T$ as a function of the GW background amplitude $\Omega_{\text{GW}}h^2$ at 0.1 Hz under the assumption that $n_T(k_{\text{CMB}}) \approx n_T(0.1\text{Hz})$ and using r_{CMB} to estimate R . Since $n_T(0.1\text{Hz}) > n_T(k_{\text{CMB}})$ by at least an order of magnitude, R departs from the expected value of one by a factor of 10 or more. The figure demonstrates that one cannot naively combine CMB tensor-to-scalar ratio with the tensor tilt at 0.1 Hz to test the consistency relation. The vertical lines mark the limits related to $\Omega_{\text{GW}}h^2$ for three of the experiments while the horizontal line $R = 1$ marks the expectation under first-order slow-roll inflation.

$\alpha_T = 0$ exactly. This large running is a reflection that the tensor tilt is largely scale dependent. Simply using the tilt at one wavenumber for the tilt at another wavenumber will lead to incorrect results. Though the running is small, the replacement of tilt at either CMB or direct detection scales with the value of the other is problematic since the two scales are largely different. While previous studies hailed the large difference in wavenumber between CMB and direct detection experiments as a “blessing” to further study inflation, for arbitrary shaped $V(\phi)$ models that are generated numerically, we find that the situation is too complex for the simple comparison. The large difference in scale requires a careful understanding of how parameters behave in between the scales, since the potentials are complicated and do not follow a power-law behavior of ϕ . And since observations are limited to two scales, making a potential reconstruction is difficult. This, however, mostly applies to the case where one is comparing observations to establish information related to an arbitrary $V(\phi)$. If one assumes a prior shape for $V(\phi)$, such as through one of the analytical models, then the behavior can be predicted analytically and the two scales can be matched to the extent that the data allow.

Instead of combining CMB and direct detection information to test the slow-roll consistency relation, perhaps, it is best to improve the measurement of $n_T(k_{\text{CMB}})$ with CMB polarization data, by improving the sensitivities so that confusing lensing B-modes are separated from primordial B-modes [35], and then using CMB data alone to study the consistency relation. On the other hand, with the feasibility of a direct detection, it is also useful to investigate if there is way to use information at direct detection frequencies for a test of inflation. Unfortunately, due to lack of information on the scalar or density perturbations at $k \sim 10^{13} \text{ Mpc}^{-1}$ it is unlikely that information on the tensor power spectrum at direct detection frequencies alone will be useful to establish slow-roll inflation. On the other hand, the complications in connecting observations to an underlying model we have outlined above may start to improve if information on scalar perturbations becomes available at a wavenumber different from that of CMB but between CMB and direct detection scales. Then there would be additional data points to interpolate between the two largely separated scales. In this respect, in an upcoming paper, we will return to such a study by concentrating on the power-spectrum of 21-cm background at $z \sim 50$ to 100 that provides information on the primordial power spectrum out to $k \sim$ a few tens Mpc^{-1} .

IV. SUMMARY

In addition to density perturbations, inflationary models of the early universe generally predict a stochastic background of gravitational waves or tensor fluctuations. By making use of the inflationary flow approach for single field models and with predictions normalized to results from cosmic microwave background and large scale structure data, we discuss the expected properties of the gravitational wave background from inflation at scales corresponding to direct detection experiments with laser interferometers in space. We complement the Monte-Carlo calculations based on the inflationary flow equations by including predictions expected under several classes of analytical inflationary models, including models involving hybrid inflation. We find that an improved version of *Big Bang Observer* (BBO-grand) can be used to detect a gravitational wave background corresponding to a tensor-to-scalar ratio above 10^{-4} at CMB scales, which is two orders of magnitude below the published goal of a tensor-to-scalar ratio of 10^{-2} by the planned next generation CMB polarization mission by NASA (*CMBpol*).

A less sensitive version of BBO (BBO-lite) with a sensitivity to gravitational waves $\Omega_{\text{GW}}h^2$ above 10^{-15} is unlikely to be useful given that the predictions suggest backgrounds well below this level when the tensor-to-scalar ratio is below 0.3. Even if the tensor-to-scalar ratio were to be above 10^{-2} , we suggest that BBO-grand will be useful to study inflationary models as standard BBO will only allow a marginal detection of the ampli-

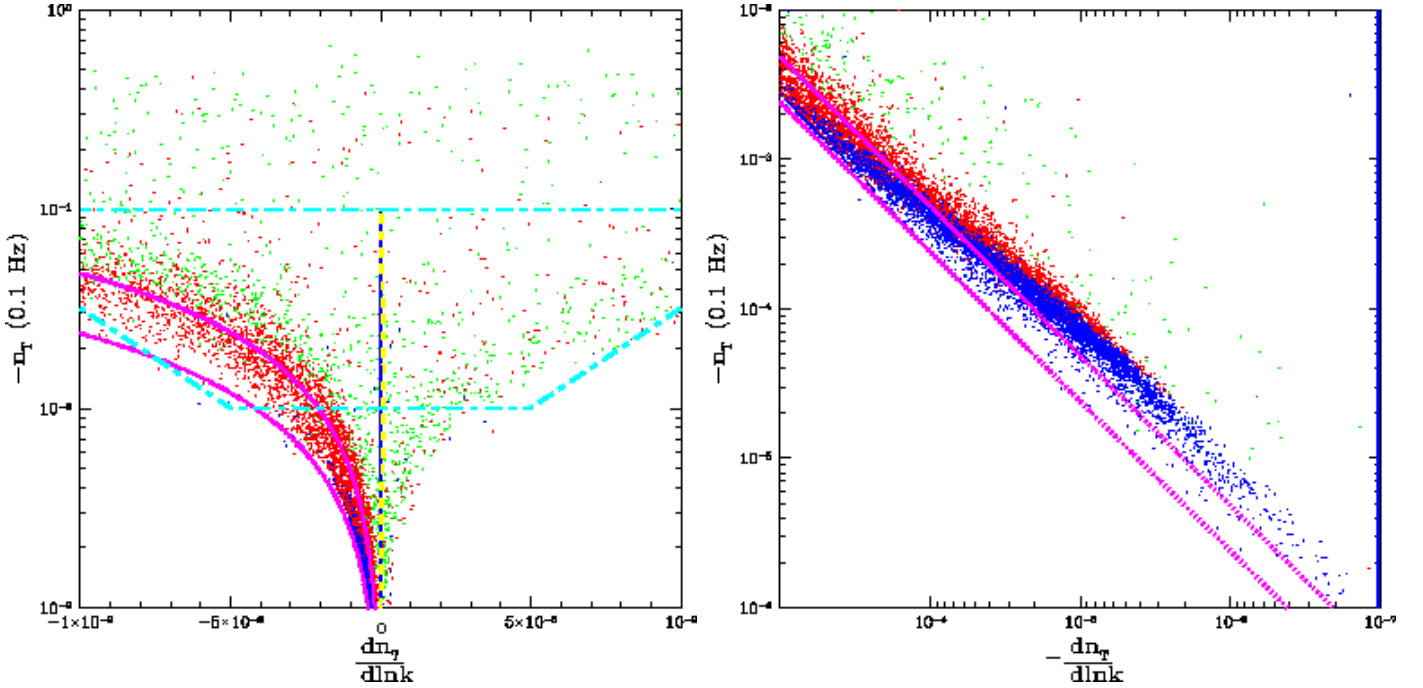


FIG. 12: The tensor spectral index n_T versus the running of the tensor tilt, α_T at 0.1 Hz. The data points show the inflationary flow predictions, while the shaded regions show the expectations under analytical model with solid, dotted, dot-dashed, and dashed lines showing power-law, chaotic, symmetry breaking, and hybrid inflation models, respectively. In certain analytical models, such as power-law, $\alpha_T = 0$ over all scales. While the left panel shows α_T in a linear scale, the right panel concentrates on the low α_T region with values around 10^{-5} .

tude while leaving the spectral index unconstrained. The polarized foregrounds, such as dust and synchrotron, are expected to limit CMB studies to a tensor-to-scalar a few times 10^{-4} , which is well above the ultimate limit of cosmic shear. Unless direct detection experiments are also affected by foreground gravitational wave sources, laser interferometers may allow us to expand the search for gravitational waves down to a tensor-to-scalar ratio of 10^{-6} .

Based on our models, we find that simple power-law approximations are not adequate to extrapolate either information at CMB scales to direct detection experiments or vice-versa. The differences are largely understood through scale dependence of the tensor tilt produced in the slow-roll inflationary models through flow equations. We also show that the simple assumption of $n_T(k_{\text{CMB}}) \approx n_T(0.1\text{Hz})$ cannot be used to establish inflationary consistency relations by combining measurements at CMB and direct detection scales. We advocate

additional measurements of the primordial scalar power spectrum at large wavenumbers beyond CMB as a way to improve model selection and predictions of inflation.

V. ACKNOWLEDGMENTS

AC and BF are supported by DOE and AM is supported by MURST through COFIN contract no. 2004027755. AC thanks members of the *Dipartimento di Fisica* and *INFN* at Universita' di Roma for hospitality while this work was initiated and participants of the "Inflation+25" conference at *Institute d'Astrophysique*, Paris for comments and suggestions that initiated this work. We thank Will Kinney, Tristan Smith, Naoki Seto, and Manoj Kaplinghat for useful discussions related to this work.

[1] D. N. Spergel *et al.* [WMAP Collaboration], *Astrophys. J. Suppl.* **148**, 175 (2003); D. N. Spergel *et al.*, arXiv:astro-ph/0603449. H. V. Peiris *et al.*, *Astrophys. J. Suppl.* **148**, 213 (2003).

[2] A. H. Guth, *Phys. Rev. D* **23**, 347 (1981); A. Albrecht and P. J. Steinhardt, *Phys. Rev. Lett.* **48** 1220 (1982); A. D. Linde, *Phys. Lett. B* **108**, 389 (1982).

[3] A. Starobinskii, *JETP Lett.* **30**, 682 (1979); L. F. Abbott and M. B. Wise, *Nucl. Phys. B* **244**, 541 (1984); A. Starobinskii, *Sov. Astron. Lett.* **11**, 133 (1985); V. A. Rubakov, M. V. Sazhin and A. V. Veryaskin, *Phys. Lett. B* **115**, 189 (1982); R. Fabbri and M. d. Pollock,

Phys. Lett. B **125**, 445 (1983); V. Sahni, Phys. Rev. D **42**, 453 (1990); B. Allen, Phys. Rev. D **37**, 2078 (1988).

[4] M. Kamionkowski, A. Kosowsky and A. Stebbins, Phys. Rev. Lett. **78**, 2058 (1997); U. Seljak and M. Zaldarriaga, Phys. Rev. Lett. **78**, 2054 (1997).

[5] G. Hinshaw *et al.*, “Three-year Wilkinson Microwave Anisotropy Probe (WMAP) observations: arXiv:astro-ph/0603451.

[6] W. H. Kinney, E. W. Kolb, A. Melchiorri and A. Riotto, “Inflation model constraints from the Wilkinson microwave anisotropy probe Phys. Rev. D **74**, 023502 (2006) [arXiv:astro-ph/0605338].

[7] R. Weiss *et al.* CMB Task Force Report, www.science.doe.gov/hep/TFCRreport.pdf

[8] M. Amarie, C. Hirata and U. Seljak, Phys. Rev. D **72**, 123006 (2005) [arXiv:astro-ph/0508293]; E. Carretti, G. Bernardi and S. Cortiglioni, arXiv:astro-ph/0609288; A. Amblard, A. Cooray and M. Kaplinghat, in preparation.

[9] L. Knox and Y.S. Song, Phys. Rev. Lett. **89**, 011303 (2002); M. Kesden, A. Cooray and M. Kamionkowski, Phys. Rev. Lett. **89**, 011304 (2002) [arXiv:astro-ph/0202434]; U. Seljak and C. M. Hirata, Phys. Rev. D **69**, 043005 (2004) [arXiv:astro-ph/0310163].

[10] E. S. Phinney *et al.* The Big Bang Observer, NASA Mission Concept Study (2003); URL <http://universe.nasa.gov/program/bbo.html>

[11] N. Seto, S. Kawamura and T. Nakamura, Phys. Rev. Lett. **87**, 221103 (2001).

[12] J. Crowder and N. J. Cornish, Phys. Rev. D **72**, 083005 (2005) [arXiv:gr-qc/0506015]; C. Ungarelli and A. Vecchio, Phys. Rev. D **63**, 064030 (2001) [arXiv:gr-qc/0003021].

[13] M. S. Turner, Phys. Rev. D **55**, 435 (1997);

[14] C. Ungarelli, P. Corasaniti, R. A. Mercer and A. Vecchio, Class. Quant. Grav. **22**, S955 (2005).

[15] T. L. Smith, M. Kamionkowski and A. Cooray, arXiv:astro-ph/0506422.

[16] T. L. Smith, H. V. Peiris and A. Cooray, Phys. Rev. D **73**, 123503 (2006) [arXiv:astro-ph/0602137].

[17] S. Chongchitnan and G. Efstathiou, Phys. Rev. D **73**, 083511 (2006) [arXiv:astro-ph/0602594]; G. Efstathiou and S. Chongchitnan, arXiv:astro-ph/0603118.

[18] A. Cooray, Mod. Phys. Lett. A **20**, (19??) [arXiv:astro-ph/0503118].

[19] M. S. Turner, M. J. White and J. E. Lidsey, Phys. Rev. D **48**, 4613 (1993) [arXiv:astro-ph/9306029]; J. R. Pritchard and M. Kamionkowski, Annals Phys. **318**, 2 (2005) [arXiv:astro-ph/0412581]; Y. Watanabe and E. Komatsu, Phys. Rev. D **73**, 123515 (2006) [arXiv:astro-ph/0604176].

[20] M. B. Hoffman and M. S. Turner, Phys. Rev. D **64**, 023506 (2001) [arXiv:astro-ph/0006321].

[21] W. H. Kinney, Phys. Rev. D **66**, 083508 (2002).

[22] R. Easther and W. H. Kinney, Phys. Rev. D **67**, 043511 (2003) [arXiv:astro-ph/0210345].

[23] J. E. Lidsey, A. R. Liddle, E. W. Kolb, E. J. Copeland, T. Barreiro and M. Abney, Rev. Mod. Phys. **69**, 373 (1997) [arXiv:astro-ph/9508078]; L. P. Grishchuk and Yu. V. Sidorav, in *Fourth Seminar on Quantum Gravity*, eds. M. A. Markov, V. A. Berezin and V. P. Frolov (World Scientific: Singapore, 1988); A. G. Muslimov, Class. Quant. Grav. **7**, 231 (1990); D. S. Sapolek and J. R. Bond, Phys. Rev. D **42**, 3936 (1990).

[24] A. R. Liddle, P. Parsons and J. D. Barrow, Phys. Rev. D **50**, 7222 (1994) [arXiv:astro-ph/9408015].

[25] A. R. Liddle, Phys. Rev. D **68**, 103504 (2003).

[26] N. Seto, arXiv:gr-qc/0510067; H. Kudoh, A. Taruya, T. Hiramatsu, and Y. Himemoto, gr-qc/0511145.

[27] Y.-S. Song and L. Knox (2003), astro-ph/0305411.

[28] L. A. Boyle and P. J. Steinhardt, arXiv:astro-ph/0512014.

[29] S. Weinberg, Phys. Rev. D **69**, 023503 (2004); S. Bashinsky, astro-ph/0505502 (2005).

[30] L. Alabidi and D. H. Lyth, JCAP **0608**, 013 (2006) [arXiv:astro-ph/0603539].

[31] S. Dodelson and L. Hui, Phys. Rev. Lett. **91**, 131301 (2003) [arXiv:astro-ph/0305113].

[32] H. Peiris and R. Easther, “Slow roll reconstruction: Constraints on inflation from the 3 year WMAP arXiv:astro-ph/0609003.

[33] G. Efstathiou and K. J. Mack, JCAP **0505**, 008 (2005) [arXiv:astro-ph/0503360].

[34] E. D. Stewart and D. H. Lyth, Phys. Lett. B **302**, 171 (1993) [arXiv:gr-qc/9302019].

[35] W. Hu and T. Okamoto, ApJ **574**, 566 (2002) [arXiv:astro-ph/0111606]; M. Kesden, A. Cooray, and M. Kamionkowski, Phys. Rev. D **67**, 123507 (2003) [arXiv:astro-ph/0302536]; C. M. Hirata and U. Seljak, Phys. Rev. D **68**, 083002 (2003) [arXiv:astro-ph/0306354].

[36] This WMAP-based normalization is higher than usual normalizations in the literature with $H/M_{\text{pl}}\sqrt{\pi\epsilon} = 10^{-5}$ [6] and generally results in a factor of a few to a ten difference between various predictions in the literature related to the amplitude of the gravitational wave background at 0.1 Hz.

[37] On a standard desktop machine, the 20 million Monte-Carlo models took about 5 days to complete. The C code to generate model predictions related to tensor and scalar power spectra using the inflationary flow equations is freely available from the authors.